https://doi.org/10.5194/bg-2019-470
Preprint. Discussion started: 3 January 2020

Biogeosciences Discussions

Organic Carbon Characteristics in Ice-rich Permafrost in Alas and Yedoma Deposits, Central Yakutia, Siberia

Torben Windirsch[1,2], Guido Grosse[1,2], Mathias Ulrich[3], Lutz Schirrmeister[1], Alexander N. Fedorov[4,5], Pavel Ya. Konstantinov[4], Matthias Fuchs[1], Loeka L. Jongejans[1,2], Juliane Wolter[1] and Jens Strauss[1]

[1]Alfred Wegener Institute Helmholtz Centre for Polar and Marine Research, Telegrafenberg A45, 14473 Potsdam, Germany
[2]University of Potsdam, Institute of Geosciences, Karl-Liebknecht-Straße 24-25, 14476 Potsdam, Germany
[3]Leipzig University, Institute for Geography, Johannisallee 19a, 04103 Leipzig, Germany
[4]Melnikov Permafrost Institute, SB RAS, 36 Merzlotnaya str., Yakutsk, Republic of Sakha, Russia, 677010
[5]BEST International Centre, North-Eastern Federal University, 58 Belinsky str., Yakutsk, Republic of Sakha, Russia, 677027

Correspondence to: Torben Windirsch (torben.windirsch@awi.de)

Abstract. Permafrost ground is one of the largest repositories of stored terrestrial natural carbon and might become a carbon source with ongoing global warming. In particular, syngenetically frozen ice-rich Yedoma deposits originating from the late Pleistocene store a large amount of carbon. This carbon has not yet become part of the recent carbon cycle. With this study of Yedoma and associated Alas deposits in Central Yakutia we aim to understand the local sediment genesis and its effect on permafrost carbon storage. For this purpose, we investigated the Yukechi Alas area (61.76495° N, 130.46664° E), a thermokarst landscape degrading into Yedoma in Central Yakutia. Two sediment cores (Yedoma upland, 22.35 m depth, and Alas basin, 19.80 m depth) were drilled in 2015. We analyzed for ice content, total carbon and total nitrogen content, total organic carbon content, stable oxygen and hydrogen isotopes, stable carbon isotopes, mass specific magnetic susceptibility, grain size distribution, and radiocarbon ages. Samples taken from both cores were radiocarbon-dated up to 50,000 years before present. The laboratory analyses of both cores revealed very low carbon contents down to several meters depth. Those core parts holding very little to no detectable carbon consist of coarser sandy material estimated to an age between 39,000 and 18,000 years before present. For this period we assume sediment input of organic-poor material. Water isotope data derived from pore ice within the Yedoma core indicate a continuously cold state of the lower core parts, thereby ruling out a potential theory of Holocene influence. In consequence, we conclude that no strong organic matter decomposition took place in the sediments of the Yedoma core until today. In contrast, the Alas core from an adjacent thermokarst basin was strongly disturbed by lake development and permafrost thaw, and accordingly its sediment and carbon characteristics differed from those of the Yedoma core. The Alas core shows homogeneous ice content and the water isotope characteristics of a slightly more decomposed organic material; the findings of very carbon-poor core sections from the Yedoma core can be duplicated. The Yedoma deposition was likely influenced by fluvial regimes in nearby streams and the Lena River shifting with climate. The low carbon content and the clear stratigraphical layering of different sediment types suggest that the Yedoma deposits in the Yukechi area differ from other Yedoma sites regarding carbon stock and sedimentological composition. We conclude that sedimentary composition and deposition regimes of Yedoma may differ significantly within the Yedoma domain. The resulting heterogeneity should be taken into account for upscaling approaches on the Yedoma carbon stock. The Alas core gives clear insights into the future development of Cenral Yakutian Yedoma deposits.

https://doi.org/10.5194/bg-2019-470
Preprint. Discussion started: 3 January 2020


Biogeosciences Discussions

1 Introduction

Permafrost deposits provide important terrestrial storage for carbon. Perennial freezing largely prevents decomposition and therefore preserves organic material. These permafrost soil conditions can be found in the ground of approximately one quarter of the Northern Hemisphere's land surface (Zhang et al., 1999). The estimated amount of frozen and unfrozen carbon stored in the terrestrial permafrost region is 1330 to 1580 gigatons (Gt) (Schuur et al., 2015), which is up to 45% more than the amount that is currently present in the atmosphere (870 Gt, using 409 ppm CO_2 measured in 2019) (Strauss et al., 2017). Permafrost formation and conservation is highly dependent on long-term climatic conditions, both directly via air temperature and indirectly by the presence or absence of insulating vegetation and snow cover (Johansson et al., 2013). Currently, these permafrost conditions are under threat by rapidly increasing global, and in particular Arctic air temperatures which have resulted in widespread permafrost warming in recent years (Biskaborn et al., 2019); a permafrost loss of up to 70% by 2100 in the uppermost 3m is expected in a business-as-usual scenario (IPCC, 2019).

A special type of permafrost is the Yedoma ice complex deposit (in the following referred to as Yedoma), formed from late Pleistocene deposition of fine-grained sediments syngenetically with large volumes of ground ice. Yedoma is ice-rich (50–90 volume percent [vol%] ice) and usually has organic carbon contents of 2 to 4 weight percent (wt%) with an estimated deposit thickness up to 40 m (Schirrmeister et al., 2013;Strauss et al., 2013;Murton et al., 2017). In the context of global climate change, such high ice content with pore ice and syngenetic ice wedges render Yedoma deposits highly vulnerable to thaw (Vonk et al., 2013). Thawing leads to ground subsidence that is associated and often combined with thaw lake development (Grosse et al., 2013). Thaw lake development, surface subsidence, lake drainage, and refreezing of formerly unfrozen thermokarst lake sediments result in a thermokarst basin landform called Alas in Central Yakutia (Soloviev, 1973). During these thaw processes, the carbon stored within the Yedoma deposits becomes exposed to decomposition in the thaw bulbs (taliks) underneath the thermokarst lakes. It is subsequently released into the atmosphere as a result of microbial activity in unfrozen and aquatic conditions, amplifying global climate change (Schuur et al., 2008). After a lake drainage event, the resulting thermokarst deposits in the Alas basins refreeze and this carbon, as well as carbon from new plant biomass forming in thermokarst lakes and basins, becomes protected from decomposition again. That these processes have occurred can usually be determined by higher carbon content and, at the same time, lower carbon stocks, compared to the adjacent deposits.

The resulting landscape patterns of Yedoma uplands and Alas basins form a heterogeneous landscape mosaic (Morgenstern et al., 2011). The heterogeneity and carbon characteristics within these deposit types, especially below 3 m, are still poorly studied. In Central Yakutia, several permafrost studies have been conducted, especially on surface dynamics and temperature changes(Fedorov and Konstantinov, 2003a;Ulrich et al., 2017a;Ulrich et al., 2017b;Ulrich et al., 2019). Other studies show a direct relation between dense vegetation cover and low permafrost carbon storage due to warmer permafrost conditions as a result of ground insulation (Siewert et al., 2015). Hugelius et al. (2014) estimate the carbon stock of permafrost in the circumarctic Yedoma region to be approximately 822 Gt carbon. However, despite the still high vulnerability of deeper deposits to thaw due to thermokarst and thermo-erosion (Turetsky et al., 2019) only very few studies report carbon

https://doi.org/10.5194/bg-2019-470
Preprint. Discussion started: 3 January 2020

characteristics for permafrost deposits deeper than 3 m. This lack of data results in very high uncertainties for the impact of deep thaw in ice-rich permafrost regions and consequences for the carbon cycle.

By investigating deeper permafrost sediments in the continuous permafrost region of Central Yakutia, we aim to understand the processes involved in organic carbon deposition and reworking in Yedoma and thermokarst deposits of this important region. Our main research questions are: (1) Which are the sedimentological processes that influenced the carbon stocks found in the Yedoma and Alas deposits of the Yukechi area? (2) How did these sedimentological processes affect the local carbon storage? We will use grain size distribution analysis, mass specific magnetic susceptibility (MS), total organic carbon (TOC) and total nitrogen (TN) analysis, and isotope measurements to identify the sedimentological processes that contributed to the formation of the Yukechi landscape. A bootstrapping approach on the measured carbon characteristics will give us estimated carbon stocks for the present deposit types and the whole area in general. This will help in predicting the future development of this landscape and the fate of its currently stored carbon.

2 Study site

The Yukechi Alas landscape (61.76495° N; 130.46664° E) covers an area of approximately 1.4 km² and is located on the Abalakh Terrace (~200 m above sea level [asl]) in the Lena-Aldan interfluve of Central Yakutia (Fig. 1a) (Ulrich et al., 2019). It is characterized by Yedoma uplands and drained Alas basins indicating active thermokarst processes (Fedorov and Konstantinov, 2003a). Yedoma deposits cover 66.4 % of the area. The lakes cover about 13.0 % of the Yukechi Alas landscape, and approximately 20.6 % of the area consists of basins covered by grasslands, which hence contain Alas deposits (Fig. S1).

Today, Central Yakutia is characterized by an extreme continental subpolar climate regime with very low winter air temperatures down to minima of -63 °C in January (Nazarova et al., 2013). Holocene climate reconstructions indicate climate settings with slightly colder conditions (T_{July} for 10,000 to 8,000 yr BP and 4,800 to 0 yr BP is 15.6 ± 0.7 °C,) compared to modern climate (T_{July} is 16.6 to 17.5 °C) and a mid–Holocene warming phase between about 6,000 and 4,500 yr BP (T_{July} ~ 1.5 °C higher than today) (Nazarova et al., 2013;Ulrich et al., 2017b). The modern Holocene mean annual air temperature (MAAT) in Siberia is -8.6 °C (Fedorov, 2006). The modern active layer thickness in Central Yakutia is approximately 1.5 m but it can be higher in grasslands, such as within Alas basins (about 2 m and more), and lower below the taiga forest (less than 1 m) (Fedorov, 2006).

Yedoma deposits in this region can be 20 to 30 m in thickness as was shown by former drilling campaigns (Soloviev, 1973). Lakes are found in partially drained basins as well as on the surrounding Yedoma uplands (Fig. 1b). The land surface within the Alas basins is covered by grasslands while the boreal forest found on the Yedoma uplands mainly consists of *Larix cajanderi* with several *Pinus sylvestris* communities (Kuznetsova et al., 2010;Ulrich et al., 2017b). Central Yakutian Alas landscapes are characterized by extensive land use (mainly horse and cattle herding and hay farming) (Crate et al., 2017).

https://doi.org/10.5194/bg-2019-470
Preprint. Discussion started: 3 January 2020

Lake dynamics have been monitored at the Yukechi Alas study site for several decades by the Melnikov Permafrost Institute in Yakutsk (Bosikov, 1998;Fedorov and Konstantinov, 2003b;Ulrich et al., 2017a) and have partially been linked to local land use (Crate et al., 2017).

Figure 1 – Study site overview; a: location of the Yukechi Alas study site in Central Yakutia on the edge of the Abalakh Terrace; b: locations of the Alas1 and the YED11 coring site within the Yukechi Alas landscape (Planet OrthoTile, acquisition date: 7 July 2018).

3 Methods

3.1 Field work

Field work took place in March 2015 during a joint Russian-German drilling expedition. Two long permafrost sediment cores were obtained, one from Yedoma deposits and one from the adjacent drained Yukechi Alas basin (Fig. 1b). The surface of the Alas sample site (61.76490° N, 130.46503° E; h = 209 m asl) is located approximately 9 m lower than the surface of the sampled Yedoma site (61.75967° N, 130.47438° E; h = 218 m asl) (Fig. 2). The distance between the two coring locations is 765 m. Both cores were drilled from dry land surface, kept frozen, and sent to the Alfred Wegener Institute (AWI) in Potsdam, Germany, for lab analysis. The Yedoma core (YED1) reached a depth of 22.35 m below surface (bs) and includes an ice wedge section from approximately 7.0 to 9.5 m bs. The Alas core (Alas1) reached 19.80 m bs. A talik section was found in the Alas core reaching from approximately 1.6 m down to 7.5 m bs.

Figure 2 – Setting of the drilling locations for the Alas1 and YED1 cores showing distance and height difference between the locations (vertical scale exaggerated).

3.2 Laboratory analyses

Laboratory work was carried out at AWI. The frozen cores were split lengthwise using a band saw and were subsequently subsampled. Each subsample consisted of approximately 5 cm core material. Subsamples were equally distributed along the cores and taken approximately every 50 cm or in order to capture the major stratigraphic layers. The samples were then weighed and thawed. Pore ice or, if previously unfrozen, pore water was extracted using artificial roots (Rhizones) consisting of porous material with a pore size of 0.1 µm. These water samples were then analyzed for stable oxygen and hydrogen isotopes (see section 3.2.5). The ice wedge ice was subsampled using a saw and also analyzed for stable oxygen and hydrogen isotopes.

3.2.1 Ice content, bulk density, and subsampling

The sediment samples were freeze-dried and weighed again for determining the absolute ice content in wt%. Ice content within talik areas represents the water content, water which froze after drilling. Bulk density was calculated from the absolute ice content, assuming an ice density of 0.9127 g/cm^3 at 0 °C and a mineral density of 2.65g/cm^3 (Strauss et al., 2012).

https://doi.org/10.5194/bg-2019-470
Preprint. Discussion started: 3 January 2020

3.2.2 Elemental analyses

Subsamples used for elemental analyses were homogenized using a planetary mill equipped with agate jars and agate marbles. Subsamples were then weighed into tin capsules and steel crucibles for the elemental analyses. Total carbon (TC), TN, and TOC content were measured via combustion and analyses of resulting gases using a vario EL III and a varioMAX C Element Analyzer. Results give the carbon and nitrogen amounts in relation to the sample mass used for analysis in wt%. The carbon nitrogen ratio (C/N) was calculated from TN and TOC. This ratio can be used as a rough indicator for the state of degradation or source of organic matter. Assuming a constant source, a higher ratio indicates better-preserved organic matter (Stevenson, 1994;Strauss et al., 2015).

3.2.3 Magnetic susceptibility and grain size analysis

Subsamples taken for grain size analysis were first measured for mass specific MS using a Bartington Magnetic Susceptibility Meter Model MS2 and a frequency of 0.465 kHz. This allows us to differentiate between different mineral compositions (Butler, 1992;Dearing, 1999).

For grain size analysis, the samples were treated with hydrogen peroxide and put on a shaker for 28 days to remove organic material. The pH was kept at a reaction-supporting level between 6 and 8. Subsequently, the samples were centrifuged and freeze–dried. One g of each sample was mixed with tetra-Sodium Pyrophosphate 10–hydrate ($Na_4P_2O_7*10H_2O$) (dispersing agent) and dispersed in an ammonia solution. The grain size distribution and proportions were finally determined using a Malvern Mastersizer 3000 equipped with a Malvern Hydro LV wet–sample dispersion unit. Statistics of the grain size measurements were calculated using Gradistat 8.0 (Blott and Pye, 2001). Results are used to identify different stratigraphic layers via material composition and to deduce sedimentary processes.

3.2.4 Radiocarbon dating

Radiocarbon dating was done for nine samples using the Mini Carbon Dating System (MICADAS) at AWI Bremerhaven. The results were calibrated using Calib 7.1 (Stuiver et al., 2018). We used bulk sediment samples for dating due to a lack of macro-organic remains within the deposits. The curve used for calibration was IntCal13 (Reimer et al., 2013) and results are given in calibrated years before present (cal yr BP). The age–depth model was developed using the "Bacon" package in the R environment (Blaauw and Christen, 2011) (Fig. S2).

3.2.5 Stable isotopes

Stable carbon isotopes can be used as a proxy for the degree of decomposition of organic material, as during decomposition and mineralization C^{12} is lost, resulting in a higher share of C^{13} and hence a higher $\delta^{13}C$ ratio (Fig. S3) (Diochon and Kellman, 2008).

Twenty-three subsamples for $\delta^{13}C$ analysis were ground and carbonates were removed by treating the samples with hydrochloric acid for three hours at 97.7 °C. The samples were then vacuum-filtered, dried, and weighed into tin capsules for

https://doi.org/10.5194/bg-2019-470
Preprint. Discussion started: 3 January 2020

analysis. The measurement of stable carbon isotopes was carried out using a Delta V Advantage Isotope Ratio MS supplement equipped with a Flash 2000 Organic Elementar Analyzer. The results are compared to the Vienna Pee Dee Belemnite (VPDB) standard and given in per mille (‰) (Coplen et al., 2006).

Stable hydrogen and oxygen isotopes can be used as a temperature proxy. Lower δ^2H and $\delta^{18}O$ values indicate a lower mean temperature; with higher temperatures evaporation increases, which leads to an increased loss of H^1 and O^{16} and raises the δ^2H and $\delta^{18}O$ ratios (Yao et al., 2006). Samples taken from ice wedges are supposed to yield a winter temperature signal, but pore ice and water signal a mix of different seasons with a higher uncertainty due to alteration and fractionation during deposition and freezing (Meyer et al., 2000).

Our δ^2H and $\delta^{18}O$ samples were measured using a Finnigan MAT Delta–S mass spectrometer and the equilibration technique was after Horita et al. (1989). In total, 29 samples were measured, of which 16 originated from YED1 pore ice, 8 originated from YED1 wedge ice, and 5 from Alas1 pore ice or pore water. The results are given in per mille related to standard mean ocean water (‰ vs. SMOW).

3.2.6 Statistics and bootstrapping approach

For the mean grain size, the median of each core unit, consisting of several samples' mean values, is given. The interquartile range of 25 % and 75 % is given.

To calculate the carbon quantity of the examined soil cores, we used a bootstrapping approach using the "boot" package in the R environment. For all TOC values below detection limit (0.1 wt%), a value of 0.05 wt% was set. Missing bulk density values, resulting from low ice contents (<20 wt%) (Strauss et al., 2012), were calculated after Eq. (1), which describes the relation between TOC and bulk density in the examined cores.

$$(1)\quad \text{bulk density} = 1.3664^{-0.115 * \text{TOC}}$$

Bootstrapping calculations were made for the sediment part of the cores. The ice wedge in YED1 was excluded in the bootstrapping. The calculations were done for separate depth levels: For the top 3 m of each core and for both complete cores with 10,000 iterations each.

For carbon budget estimations of the Yukechi Alas area, the core length of the examined cores was assumed to represent the different ground types, resulting in a general depth of 22 m for Yedoma deposits and 20 m for Alas deposits. A mean wedge-ice volume of 46.3 % for Central Yakutian Yedoma deposits and 7 % for Alas deposits of Central Yakutia was assumed following Ulrich et al. (2014).

https://doi.org/10.5194/bg-2019-470
Preprint. Discussion started: 3 January 2020

4 Results

4.1 Characteristics of the Yedoma deposits

The Yedoma core YED1 visually appears rather heterogeneous (Fig. 3a) with material varying from fine gray material (Fig. 3b[1]) to sandy grayish brown material (Fig. 3b[2]). Between 0 and 691cm bs and between 1920 and 2235 cm bs, brown to black dots up to 2 cm in diameter may be organic-rich material. Cryostructures include structureless to micro-lenticular ice and larger ice veins and bands. The core penetrated an ice wedge between 691 and 1005 cm bs, in which only ice but no sediment samples could be collected. The core contains an unfrozen layer close to the surface between approximately 100 and 200 cm bs, representing a thin initiating talik layer underneath the 100 cm thick frozen active layer (Fig. 3a, red). Taliks form because the active layer does not freeze completely anymore in some regions.

Figure 3 – a: overview of the Yedoma core; depth given in cm bs; state after core retrieval is given by colors: blue = frozen, red = unfrozen; location of the ice wedge is marked; brown marks silty sediments, yellow marks sandy sediments; b: detailed pictures of the YED1 core; (1) 317-332 cm bs, picture of Y1 showing black organic-rich inclusions within the grey silty matrix; (2) 1532-1549 cm bs, picture of Y3, showing the coarse sandy material with no visible cryostructures or organic material.

We divided the Yedoma core into four main Yedoma units (Y) (Fig. 4). Y4 is the lowest (2235 to 1920 cm bs) and oldest (radiocarbon age of 49,323 cal yr BP) stratigraphical unit. The absolute ice content slightly increased towards the surface (35.8 to 36.6 wt%, peak value of 53.6 wt% in between). MS also increased from 60.726 to 155.359 * 10^{-8} m^3/kg. The grain size was rather consistent with a median value of $25.3^{+0.9}_{-0.7}$ µm and the material composition varied between sand and silt (Fig. S4, S5). TOC contents of up to 1.7 wt% (mean of 1.3 wt%) were found. The C/N ratios within this unit varied between 9.2 and 10.6, and $\delta^{13}C$ values ranged between -25.27 and -24.66 ‰ vs. VPDB (Fig. S3).

Y3 (between 1927 and 1010 cm bs) was dated with an infinite radiocarbon sample. There is a transition zone between Y4 and Y3 represented by a diagonal sediment boundary in the core between 1927 and 1920 cm bs (see Fig. 3a). Y3 showed distinctly lower absolute ice contents (< 32.1 wt%). MS varied between 120.468 and 285.023 * 10^{-8} m^3/kg. Higher sand contents (> 56.9 vol%) led to an increase in mean grain size (72.1 to 191.6 µm); grain size only decreased down to 33.3 µm in the uppermost sample of Y3. No measurable TOC was found in this unit.

Y2 (1010 to 714 cm bs) consisted of ice-wedge ice. Thus, only δ^2H and $\delta^{18}O$ were measured and are described in section 4.3.

Y1 (714 to 0 cm bs) is the youngest unit with carbon ages ranging between 40,608 (589.5 cm bs) and 21,890 cal yr BP (157.5 cm bs). Ice content decreased from the ice wedge towards the surface. Values ranged from 14.6 wt% (110 cm bs) to 57.4 wt% (688 cm bs). MS decreased towards the surface ranging from 108.12 * 10^{-8} m^3/kg to 15.36 * 10^{-8} m^3/kg in the uppermost sample, with a maximum of 118.63 * 10^{-8} m^3/kg at 298 cm bs. This unit consisted of fine sediment with a median grain size

https://doi.org/10.5194/bg-2019-470
Preprint. Discussion started: 3 January 2020

of $20.3^{+0.9}_{-2.2}$ µm. It contains up to 1.4 wt% TOC (298 cm bs). C/N values were in the range of 9.1 to 12.9. The lowest $\delta^{13}C$ value was found at 21 cm bs with -28.07 ‰ vs. VPDB; the lower part of this section showed a mean value of -24.42 ± 0.6 ‰ vs. VPDB.

Figure 4 - Characteristics of the Yedoma core YED 1: radiocarbon age, absolute ice content, bulk density, MS, grain size composition, mean grain size, TOC, C/N ratio and $\delta^{13}C$ ratio; hollow triangle indicates an infinite radiocarbon age; grey/white areas mark the different stratigraphic units (Y1 to Y4).

The cumulative grain size results (Fig. S5) illustrate the differences between the core units. Silt is the dominant grain size class in Y4 and Y1, whereas unit Y3 is clearly dominated by sand.

Our results reveal only small amounts of TOC in the Yedoma deposit. The TOC values were smaller than 0.1 wt% in 24 of 36 samples. Y3 contained no detectable TOC.

The calibrated radiocarbon ages of the Yedoma deposits are listed in Table 1 and assigned to the different core units. Our age–depth model (Fig. S2a) indicates a steep age-depth relationship from approximately 1200 to 2235 cm bs and a rather well defined, gradual age-depth relationship from 1200 cm bs towards the surface (Fig. S2a).

The bootstrapping approach resulted in a mean soil organic carbon (SOC) estimation of 4.48 ± 1.43 kg/m³ for the top 3 m of the YED1 core and a mean of 5.27 ± 1.42 kg/m³ for the entire core. We calculated a carbon inventory of 56.8 ± 15.2 kt for the Yukechi Yedoma by upscaling the carbon storage to the complete Yedoma coverage in the Yukechi Alas landscape (66.4 %, ~ 917,000 m²) (Fig. S1). In this calculation we assumed a Yedoma thickness of 22 m, similar to the length of the YED1 core, and we used the average TOC densitiy of YED1 (5.27 kg/m³).

4.2 Characteristics of the Alas deposits

The Alas1 core contains a large proportion of unfrozen sediment (i.e. talik; ~ 160 to 750 cm bs) (Fig. 5a, red), which led to the loss of some core sections during drilling. The absolute ice content given for samples retrieved from this zone represents absolute water content; samples were frozen directly after core recovery and field description. The core's visual appearance was more homogeneous compared to YED1 regarding color (greyish brown) and material (clayish silt [Fig. 5b(1)] to sandy silt [Fig. 5b(2)]). Cryostructures of the frozen core below 750 cm bs included horizontal ice lenses up to 5 cm thickness and structureless non-visible ice. Blackish dots and lenses (up to 1 cm in diameter) hint that organic material is included in the sediments. We estimated the active layer to reach down to approximately 200 cm bs based on Fedorov (2006).

Figure 5 – a: overview of the Alas1 core; depth given in cm bs; state after core retrieval is given by colors: blue = frozen, red = unfrozen; light brown marks silty material, yellow marks sandy material, dark brown marks silty material containing more organic material; b: detailed pictures of the Alas1 core; (1) 828–840 cm bs picture of the sandy A2 unit; (2) 1767–1781 cm bs picture of the fine-grained silt-dominated A4 unit including black organic-rich inclusions.

https://doi.org/10.5194/bg-2019-470
Preprint. Discussion started: 3 January 2020


Biogeosciences Discussions Open Access EGU

We divided the Alas1 core into four stratigraphic units (A1 to A4), according to cryolithologic composition and carbon content (Fig. 6). The oldest unit is A4 (1980 to 1210 cm bs) with radiocarbon ages of 42,865 cal yr BP (1967.5 cm bs) and 45,870 cal yr BP (1530.5 cm bs). An age inversion was detected here. Absolute ice content was rather stable and ranged from 15.3 wt% at 1400.5 cm bs to 25.4 wt% at 1220 cm bs. MS ranged between 62.146 * 10^{-8} m^3/kg (1967.5 cm bs) and 133.930 * 10^{-8} m^3/kg (1759 cm bs) with much higher values in the sand intrusion (266.667 * 10^{-8} m^3/kg at 1464 cm bs, 268.690 * 10^{-8} m^3/kg at 1400.5 cm bs). The mean grain size was rather constant (median of $27.4^{+3.6}_{-10.0}$ µm) except for a sandy intrusion between 1530.5 and 1312 cm bs (152.9 µm at 1464 cm bs, 72.6 µm at 1400.5 cm bs) (Fig. S4, S6). While TOC values were below detection limit within this sandy material, the other parts of A4 held TOC amounts of up to 1.8 wt% (1759 cm bs). The C/N ratio ranged between 5.8 (1274 cm bs) and 8.9 (1759 cm bs) with a mean value of 7.4 (Fig S2). The $\delta^{13}C$ values showed a range of -25.67 to -24.06 ‰ vs. VPDB (Fig. S3).

A3 ranged from 1210 to 925 cm bs. The absolute ice content was stable around 22.7 ± 2.9 wt%. MS increased towards the surface from 72.102 * 10^{-8} m^3/kg (1205.5 cm bs) to 122.629 * 10^{-8} m^3/kg (955 cm bs). A3 was characterized by less coarse material compared to A4, with a median grain size of $20.4^{+5.1}_{-3.2}$ µm. All TOC values were below detection limit, so no C/N could be calculated and no $\delta^{13}C$ could be measured.

The characteristics of A2 (925 to 349 cm bs) were similar to those of the sand intrusion found in A4. A radiocarbon age of 27,729 cal yr BP was measured at 812.5 cm bs. The absolute ice content had a mean value of 15.2 wt% and decreased from 16.7 wt% at 919.5 cm bs to 12.9 wt% at 395 cm bs. MS decreased upwards from 302.337 to 129.232 * 10^{-8} m^3/kg. The mean grain size at the bottom of this unit was 102.3 µm (919.5 cm bs), increased to 221.9 µm at 812.15 cm bs towards the surface, and reached the lowest value of 41.2 µm at the upper boundary of A2. All TOC values were below the detection limit.

The uppermost stratigraphic unit A1 starts at 349 cm bs. It is the youngest unit of Alas1 with a radiocarbon sample at 199 cm bs dated to 15,287 cal yr BP. The absolute ice content slightly increased from 19.1 wt% (344.5 cm bs) to 23.1 wt% (9 cm bs) throughout this unit. MS decreased towards the surface, starting at 126.692 * 10^{-8} m^3/kg (344.5 cm bs) and reaching 50.772 * 10^{-8} m^3/kg at 9 cm bs. The mean grain size decreased again, compared to A2, representing silty material with values of $18.5^{+1.4}_{-1.6}$ µm. TOC was only detectable in the uppermost sample with a value of 2.4 wt% (9 cm bs). The C/N ratio for this sample was 12.0 and the $\delta^{13}C$ was -27.24 ‰ vs. VPDB.

Figure 6 - Characteristics of the Alas1 core: radiocarbon age, absolute ice content, bulk density, MS, grain size composition, mean grain size, TOC, C/N ratio and $\delta^{13}C$ ratio; grey/white areas mark the different stratigraphic units (A1 to A4).

The radiocarbon ages are listed in Table 1. The age-depth model (Fig. S2b) shows a rather continuous steepness for all calibrated ages of Alas1.

https://doi.org/10.5194/bg-2019-470
Preprint. Discussion started: 3 January 2020

Bootstrapping resulted in a mean SOC value of 6.93 ± 2.90 kg/m³ for the top 3 m of the Alas1 core. The calculation for the whole core resulted in a mean value of 6.07 ± 1.80 kg/m³ carbon. For the whole Alas area within the Yukechi Alas landscape (20.6 %, ~ 284,000 m²) (Fig. S1 [green]), we calculated a total organic carbon stock of 32.0 ± 9.6 kt.

4.3 Water isotope analysis of the YED1 and Alas1 core

Stable hydrogen and oxygen isotope results are shown in figure 7. There was a clear downward trend of $\delta^{18}O$ values becoming more negative between 400 and 1000 cm bs in the YED1 core (Fig. 7b). It was shown that lower $\delta^{18}O$ values are linked to lower $\delta^{2}H$ values (Fig. S7), as there was a downward trend of $\delta^{2}H$ values over depth in this core section as well. Below 1000 cm bs, both $\delta^{2}H$ and $\delta^{18}O$ become less negative with increasing depth. $\delta^{18}O$ ranged between -25.16 ‰ at the lowermost sample and -30.70 ‰ at 1071.5 cm bs with a much less negative value of -15.53 ‰ closest to the surface. While the uppermost Yedoma sample had a $\delta^{2}H$ value of -120.8 ‰, all other Yedoma samples showed much more negative values between -181.3 ‰ (2209.5 cm bs) and -221.6 ‰ (1071.5 cm bs). Values almost aligned with the global meteoric water line (GMWL) and the local evaporation line (LEL) of Central Yakutia (Wetterich et al., 2008), except for the ice wedge samples of YED1 (Fig. 7a). The isotope data obtained from the ice wedge samples had more negative values for both $\delta^{2}H$ (-220.6 ‰ to -228.6 ‰) and $\delta^{18}O$ (-29.58 ‰ to -30.55 ‰) in comparison to the remaining YED1 core.

Most of the Alas samples were too dry to extract pore water for water isotope analysis, resulting in a low number of water samples for this core (Fig. 7c). These Alas1 samples showed less variance in $\delta^{2}H$ and $\delta^{18}O$ data, ranging from -13.33 ‰ (103 cm bs) to -15.48 ‰ (1154 cm bs) for $\delta^{18}O$ and -130.4 ‰ (61 cm bs) and -137.6 ‰ (1464 cm bs) for $\delta^{2}H$.

Figure 7 – The characteristics of water stable isotopes in the studied sediment cores. a: stable hydrogen and oxygen isotope ratios of YED1 pore ice (black triangles), YED1 ice wedge ice (semi-hollow triangles), and Alas1 pore ice and pore water (black dots) [‰ vs. SMOW]; global meteoric water line GMWL: y=8x; local evaporation line LEL of Central Yakutia (based on data compiled until 2005 after Wetterich et al., 2008); b and c: oxygen isotopes of YED1 (b) and Alas1 (c) plotted over depth.

5 Discussion

5.1 Carbon accumulation and loss at the Yukechi study site

We found surprisingly low TOC values in the Yedoma and Alas deposits. These low values appear in correlation with coarser sediments (fine sand), while the rather fine sediment layers (silt and sandy silt) store more TOC. The similarities in sediment structure and composition of the two cores and the increased accumulation rates towards the core bottoms (Fig. S2) indicate that the sedimentary regime was the same for both cores until approximately 35,000 cal yr BP (Fig. 4 and 6).

https://doi.org/10.5194/bg-2019-470
Preprint. Discussion started: 3 January 2020

On the one hand, low TOC content could be a result of high organic matter decomposition during accumulation or during a thawed state, especially in thermokarst deposits. On the other hand, it could simply reflect low input. In our case, we argue that the stable carbon isotope data of our cores, assuming that the source signal was more or less constant with time, are between -24.06 and -27.24 ‰ and are at the low end, but comparable to other studied sites from the Yedoma domain (Schirrmeister et al., 2013;Strauss et al., 2013;Jongejans et al., 2018). Both cores show the lowest $\delta^{13}C$ values closest to the surface as the organic material is the most recent and therefore least decomposed. As we look deeper in the cores, $\delta^{13}C$ becomes less negative and constant with depth in the Alas and Yedoma deposits; we interpret this to mean greater decomposition at depth. Decomposition ceased when the lower samples became frozen, resulting in a constant $\delta^{13}C$ at depth. The stable C/N ratios in both cores support this hypothesis and are in line with the results found by Strauss et al. (2015) and Weiss et al. (2016). In comparison to the mean C/N ratio of 10 in YED1, the mean C/N ratio of 8 for Alas1 may indicate that the Alas deposits were only slightly more affected by decomposition. As the carbon was freeze-locked in the YED1 core and therefore was not decomposed since deposition, this similarity in mean C/N ratios indicates that the original carbon state for the deposits at both coring sites were similar, assuming the same carbon source for both deposits. The slightly lower C/N values found in Alas1 likely resulted from decomposition well after original deposition. It is more likely that the initiation of a talik led to increased decomposition of these sediment sections.

The Yukechi C/N values are on the low end of C/N ratios known from other Yedoma deposits, e.g. from Bykovsky Peninsula (Schirrmeister et al., 2013) and Duvanny Yar (Strauss et al., 2012). The similarity of the low C/N ratios from both cores supports the hypothesis of input of organic-poor and already decomposed material rather than the complete post-deposition decomposition of the organic matter in the now organic-free core segments, as the latter would require unfrozen conditions for extended periods in deep layers at the coring sites.

We found age inversions in both cores at similar age and depth (YED1 49,232 cal yr BP, 1998.5 cm bs; Alas1 42,865 cal yr BP, 1967.5 cm bs) (Fig. 4 and 6, Fig. S2). The stable water isotopes signal of YED1 shows characteristics different from precipitation water or the Alas1 water isotope results throughout the core (Fig. 7, Fig. S7) which is evidence that YED1 has not been thawed since accumulation. Rather, these findings suggest a temporary shift in sediment input at approximately 35,000 cal yr BP. This would have been caused by reworking of sediments or the remobilization of older material by transport processes and the incorporation of this older material in younger sediments.

The permanently frozen conditions of the Yedoma deposits at YED1 are supported by the water isotope signals (Fig. 7) with much lower $\delta^{18}O$ values for the lower Yedoma pore ice, compared to the uppermost sample showing a water isotope signal of very recent climate. If the Yedoma core had been thawed at some point, intruding water would have led to a rather homogeneous oxygen isotope signal throughout the core. This e.g. can be seen in the Alas core. Also, the intact ice wedge supports the hypothesis of a permanently frozen state throughout the depositional history at YED1. The very similar isotope signals derived from the ice wedge indicate even colder climate conditions during the formation of that ice wedge. Brosius et

https://doi.org/10.5194/bg-2019-470
Preprint. Discussion started: 3 January 2020

al. (2012) show similar δ^2H and $\delta^{18}O$ values in Central Yakutia for an ice wedge dating to late Pleistocene (-242 ‰ for δ^2H and -30.9 ‰ for $\delta^{18}O$). The offset in comparison to the ice wedge we examined can be explained by climatic variations. The negative trend in the $\delta^{18}O$ values of YED1, starting from the bottom towards the ice wedge, is likely linked to a cooling climate in Central Yakutia from approximately 49,000 to 41,000 cal yr BP (Fig. 7b).

These findings indicate that the low carbon content must result from low carbon input rather than high decomposition rates in both cores, as no evidence for conditions favoring high decomposition rates was found. Furthermore, the very similar sediment characteristics of both cores suggest that the Alas deposits originate from in situ thaw and reworking of the local Yedoma. Therefore, low carbon content is likely not the result of high decomposition rates during lake coverage. For this scenario, organic carbon parameters would differ largely in carbon content and isotope signature from those of the still-frozen Yedoma (Walter Anthony et al., 2014).

The age-depth models of both cores show steep curves, hence higher sedimentation rates at the bottom of both cores, which slow down towards the surface (Fig. 4 and 6, Fig. S2). This indicates that during the early phase of the sediment accumulation (~ 45,000 to 35,000 cal yr BP) the depositional environment at Alas1 was the same as at YED1. The steepness of the age–depth model suggests an upward decrease in the accumulation rate, or can be interpreted as an increase in surface erosion towards the top of the YED1 core (Figure S3a). Especially the sandy core part of Y3 accumulated quickly with the next radiocarbon sample below dated to 49,232 cal yr BP (71.5 cm below the bottom of Y3) and the next radiocarbon sample above dated to 40,608 cal yr BP (420 cm above the top of Y3). These 917 cm of Y3 therefore accumulated in less than 8,624 years, while in Y1, the accumulation of 714 cm took more than 18,718 years (40,608 cal yr BP at 589.5 cm bs, 21,8900 cal yr BP at 157.5 cm bs) (Table 1). The continuous steepness shown by the age-depth model of Alas1 (Fig. S2b) suggests a rather stable accumulation rate throughout the deposition of these sediments.

5.2 Yedoma and Alas coherence

The differences in ice content between both cores and the homogeneity of ice content throughout the whole Alas1 core indicate that the Alas deposit was influenced by thaw processes. This is underlined by the water isotope signals which are quite homogeneous throughout Alas1, suggesting that these deposits previously thawed under thermokarst influence and were in a state of meltwater saturation in a talik. Subsequent talik refreezing resulted in structureless pore ice, forming a taberal deposit (Wetterich et al., 2009). This is a result of percolating surface water during a thawed state. The saturation with surface water results in homogeneous isotope signals throughout thawed core segments. Refreezing starting from the surrounding frozen ground rather than from the surface, as a talik is still present in the upper core part, resulted in structureless, invisible to microlenticular ice structures, due to the sandy material providing relatively large pore spaces (French and Shur, 2010). Due to the formation of those small ice structures, no sediment was moved here by the formation of e.g. large ice veins, resulting in an unmixed and still clearly structured sediment, including the contained carbon (Iwahana et al., 2014). This also excludes cryoturbational processes as an explanation for the age inversions that we found.

https://doi.org/10.5194/bg-2019-470
Preprint. Discussion started: 3 January 2020

Taking into account that there are core units with coarse material and very little organic carbon (i.e. Y3 and A2, see Fig. 4 and 6) that alternate with finer and more carbon-rich material (i.e. Y1 and Y4 in Fig. 4, A4 in Fig. 6), there must have been shifts in the sedimentary regime at the Yukechi study site (Soloviev, 1973;Ulrich et al., 2017a;Ulrich et al., 2017b). Due to the great thickness of the layers (core units 1 to 4, Fig. 4 and 6) the most suitable explanation is material transport by tributaries on top of the (former) Yedoma uplands of the Abalakh Terrace. Tributary paths changed over time, resulting in flooding connections to and then disconnections from our study area. During the river-connected flooding times at our study site, the sandy material was deposited. Fluvial transport gives a suitable explanation for absent carbon as organic matter decomposition is often much higher under aquatic conditions (Cole et al., 2001). High flow velocity also plays an important role in deposition processes, as higher flow velocities allow for larger particles to be deposited but keep the lighter organic material in suspension (Anderson et al., 1991;Wilcock and Crowe, 2003;Reineck and Singh, 2012).

Another explanation for the occurrence of these carbon-poor sandy layers are shifts in wind direction and wind speed and therefore the sediment carrying capacity of the wind (Pye, 1995). A shift in eastern Siberian climate during the beginning of the Karginian interstadial (MIS 3, ~ 50,000 yr BP) resulted in higher winter temperatures (Diekmann et al., 2017) and therefore higher pressure gradients within the atmosphere, leading to greater wind speeds. That in turn resulted in higher sediment carrying capacity of the wind and would provide a suitable explanation for the sediment differences. Also, sand dunes of the Lena River valley (Huh et al., 1998) could have provided sufficient sandy material throughout the formation of the sand layers found in the Yukechi deposits (Y3 and A2 in Fig. 4 and 6). The radiocarbon ages of these coarser core segments (Y3 and A2 in Fig. 4 and 6) dated between 39,000 and 18,000 cal yr BP match the timing of these climatic changes. Increasing wind speeds at the beginning of a warmer interstadial phase during the MIS 3 (Karginian climate optimum, 50,000 to 30,000 yr BP) and a subsequent decrease in wind speed during the cooler stadial MIS 2 are a suitable explanation (Diekmann et al., 2017). Those increased wind speeds could have led to further transport of the coarser material from the source area, enabling these materials to reach our study area (Anderson et al., 1991). Under such conditions the fine and organic-bearing material would have been deposited even farther away (Pye, 1995).

However, because of the thickness of these sandy layers of up to 10 m, continuous fluvial deposition is more likely than continuous aeolian deposition over several thousand years. In our opinion, the deposition period of approximately 7000 yr and the lack of organic material indicates fluvial deposition.

We believe that periodic flooding events of Lena River tributaries near our study area are more likely. The original Yedoma deposits of the Yukechi area were most likely formed by seasonal alluvial flooding, depositing silty sediment and small portions of organic material. The climatic changes (Diekmann et al., 2017) and the resulting higher water availability during the dated deposition period of the sandy layers may have caused changes in fluvial patterns on the Abalakh Terrace. More water could cause greater flow velocities under warmer climatic conditions and therefore increased erosive power, leading to the formation of new flow channels (Reineck and Singh, 1980). The increased flooding frequency combined with greater flow

https://doi.org/10.5194/bg-2019-470
Preprint. Discussion started: 3 January 2020

velocities resulted in the sedimentation of more coarse, sandy material (Wilcock and Crowe, 2003), while lighter organic material and silt were kept suspended and transported further, out of the Yukechi area. With a climatic backshift to colder conditions during MIS 2 water availability decreased, and silty organic-bearing material was deposited by seasonal flooding again on top of the sandy layers. This likely led to lake initiation on top of the Yedoma deposits. The underlying ground began to thaw (Grosse et al., 2013), forming the Yukechi Alas basin. As a result, ice was lost from the sediment and the ground subsided by at least 9 m (see section 3.1, height difference of 9 m between YED1 and Alas1 surface). Surface or lake water was able to percolate through the unfrozen sediments, as visible in the water isotope signal (Fig. 7, Fig. S7). Under the unfrozen aquatic conditions in the sediment, microbial activity started, resulting in the decomposition of the already small amount of organic material (Cole et al., 2001). When the lake drained, the sediment started to refreeze both upward from the underlying permafrost and downward from the surface, leaving a talik in between (Fig. 5). The subsided ground indicates that core unit A4 (Fig. 6) lies beneath the lowest unit of the Yedoma core, Y4 (Fig. 4), while units A1 to A3 shrank due to thawing from approximately 2200 to 1200 cm length. This might represent the future path of the Yukechi Yedoma deposits, as already an initiating talik of approximately 150 cm was found at the YED1 site (Fig. 3a). This is caused by ground temperature warming which itself is affected by snow layer thickness and air temperatures and more, and could lead to Alas development (Ulrich et al., 2017a). Maybe a tipping point at YED1 towards the development of characteristics similar to those found at Alas1 has already been passed.

5.3 Central Yakutian Yedoma deposits in a circumarctic and regional context

Strauss et al. (2017) calculated a mean organic carbon density for the upper 3 m of Yedoma deposits in the Lena-Aldan interfluve of 25 to 33 kg/m^3. Using a bootstrapping approach after Jongejans et al. (2018), based on our measured values we found a much lower organic carbon density of 4.48 ± 1.43 kg/m^3 for the top 3 m of the YED1 core. For Alas1, an organic carbon density of 6.93 ± 2.90 kg/m^3 was calculated for the top 3 m. This results in a mean organic carbon density of only 4.40 kg/m^3 for the top 3 m of dry soil at the Yukechi study site. This means that both our Yukechi site average and our individual cores are substantially below the range (25 to 33 kg/m^3) measured by Strauss et al. (2017). This strong difference between previously published and our new data from the same region can only be explained by high depositional heterogeneity of the Central Yakutian permafrost landscapes that was not represented in the earlier dataset of Strauss et al. (2017) in sufficient detail. Findings of Siewert et al. (2015) also differ greatly from our findings at the Yukechi site, showing carbon densities of approximately 19.3 kg/m^3 for the top two meters of larch forest-covered Yedoma deposits and approximately 21.9 kg/m^3 for the top two meters of grassland-covered Alas deposits in a setting similar to the Yukechi site (Spasskaya Pad/Neleger site) . However, with our low-carbon site we are reporting the first carbon stock estimation for Central Yakutian Yedoma deposits below 3 m.

In general, Yedoma deposits are estimated to hold 14 ± 8 kg/m^3 organic carbon in the top 3 m (Strauss et al., 2012) and 19 +13/-11 kg/m^3 for the whole column within the Pleistocene Yedoma deposits (approximate depth of 25 m) (Strauss et al., 2013). Jongejans et al. (2018) calculated a slightly larger organic carbon stock of 15.3 ± 1.6 g/m^3 for Yedoma deposits found

https://doi.org/10.5194/bg-2019-470
Preprint. Discussion started: 3 January 2020

on the Baldwin Peninsula in Alaska. Another study by Shmelev et al. (2017) stated a Yedoma carbon stock of 14.0 ± 23.5 kg/m³ for a study region in northeastern Siberia between the Indigirka River and the Kolyma River.

Assessing the carbon inventory of the full-length Central Yakutian cores examined in this study, we estimated an organic carbon density of 5.27 ± 1.42 kg/m³ for the sediments of the YED1 core down to a depth of 22.12 m bs, excluding the ice wedge. The organic carbon density at this site is approximately four times lower than estimated in previous studies of deep Yedoma deposits (Strauss et al., 2012;Shmelev et al., 2017;Jongejans et al., 2018). This also shows that, even when including roughly 10 m of organic carbon-free material, large portions of organic carbon must be stored below 3 m, as the organic carbon density increases from measurements of the top 3 m to measurements of the whole core. The Alas1 core contains slightly more organic carbon with a mean value of 6.07 ± 1.80 kg/m³ organic carbon for the whole core (19.72 m). Within the Alas core, organic carbon storage is slightly higher in the top 3 m (~ 14 % more than below). This might result from former lake coverage and the related accumulation of organic material.

6 Conclusions

In our study, we investigated two deep permafrost sediment cores from a Yedoma upland and an Alas basin in the Central Yakutian Yedoma region. Concerning our first research question, 'Which are the sedimentological processes that influenced the carbon stocks found in the Yukechi area?' we conclude the following: Low organic carbon contents are not caused by high organic matter decomposition but rather originate from the accumulation of organic-poor material during the late Pleistocene MIS 3 and MIS 2 periods. The most likely scenario is the temporary existence of tributary rivers on the Abalakh Terrace, with high flow velocities and alternating paths as a result of climatic changes, and differences in sedimentation as a result.

Concerning our second research question, 'How did these sedimentological processes effect the local carbon storage?' we show that the Yedoma deposits contained in these cores, down to a depth of 22 m, are characterized by low organic carbon contents, often less than 1 wt% TOC, resulting in a mean C storage of ~ 5 kg/m³. These low organic carbon contents are not caused by high organic matter decomposition rates but rather originate from the accumulation of organic-poor material during the late Pleistocene (MIS 3 and MIS 2 periods). This is corroborated by very similar findings in the examined Alas core.

As a result, the studied Yukechi Yedoma deposits store less carbon than other, comparable Yedoma Ice Complex deposits in the Central Yakutian area. The biogeochemical impact of permafrost thawing in the Yukechi area might therefore be smaller than generally assumed for Yedoma deposits, as this area does not feature the high carbon stock estimates of other previously studied localities in Central Yakutia and elsewhere in the Arctic.

Nevertheless, the high ice content and the presence of ice wedges make these deposits vulnerable to deep thaw processes, which will result in further ground subsidence and hence landscape changes (e.g. evolution of thermokarst lakes, infrastructure damage, etc.). Recent ongoing degradation was detected on the Yedoma upland, where the winter season temperatures are no longer cold enough to refreeze the active layer completely anymore. This phenomenon could be widespread in the sub-Arctic.

https://doi.org/10.5194/bg-2019-470
Preprint. Discussion started: 3 January 2020

The permafrost characteristics found in the Alas core reveal that its composition and stratigraphy before lake formation and drainage was very similar to the Yedoma core material. Its past development of thaw, the loss of old ice, and surface subsidence, along with sediment compaction, shows a possible pathway for the Central Yakutian Yedoma deposits under the influence of global climate change.

Data availability

The measurement data and laboratory results are available via PANGAEA at https://doi.org/10.1594/PANGAEA.898754 (Windirsch et al., 2019).

Supplement link

Author contribution

JS designed the study concept. TW conducted the laboratory work, analyzed the laboratory results, prepared the graphics, and led the writing of this paper. GG and AF led the drilling expedition in 2015. JS, MU, and PK participated in the drilling fieldwork. GG and JS supervised the data analyses and provided expertise on thermokarst processes and cryostratigraphy. LS provided expertise on grain-size characteristics and Central Yakutian permafrost genesis. MF designed the maps and provided expertise on Yedoma and thermokarst-affected carbon. LJ developed the bootstrapping routine and provided expertise on carbon stock upscaling. JW developed the age-depth models and worked on age calibration and contextualization. JS took part in the laboratory work and provided expertise in permafrost carbon processes. All authors contributed to commenting and editing the manuscript.

Competing interests

The authors declare no conflict of interest.

Acknowledgements

This study is based on a joint field campaign of the ERC PETA-CARB project (Starting Grant #338335) and the DFG project UL426/1-1 and was carried out in cooperation with the Melnikov Permafrost Institute, Siberian Branch of Russian Academy of Sciences. TW was funded by the PoGS and LJ was funded by the DBU. The field campaign was supported by Avksentry P. Kondakov. We thank Dyke Scheidemann (Carbon and Nitrogen Lab [CarLa]) and Mikaela Weiner (Stable Isotope Lab) from AWI for assistance in the laboratory.

References

Anderson, R. S., Sørensen, M., and Willetts, B. B.: A review of recent progress in our understanding of aeolian sediment transport, Aeolian Grain Transport 1, 1-19, 1991.

https://doi.org/10.5194/bg-2019-470
Preprint. Discussion started: 3 January 2020

Biskaborn, B. K., Smith, S. L., Noetzli, J., Matthes, H., Vieira, G., Streletskiy, D. A., Schoeneich, P., Romanovsky, V. E., Lewkowicz, A. G., Abramov, A., Allard, M., Boike, J., Cable, W. L., Christiansen, H. H., Delaloye, R., Diekmann, B., Drozdov, D., Etzelmüller, B., Grosse, G., Guglielmin, M., Ingeman-Nielsen, T., Isaksen, K., Ishikawa, M., Johansson, M., Johannsson, H., Joo, A., Kaverin, D., Kholodov, A., Konstantinov, P., Kröger, T., Lambiel, C., Lanckman, J.-P., Luo, D., Malkova, G., Meiklejohn, I., Moskalenko, N., Oliva, M., Phillips, M., Ramos, M., Sannel, A. B. K., Sergeev, D., Seybold, C., Skryabin, P., Vasiliev, A., Wu, Q., Yoshikawa, K., Zheleznyak, M., and Lantuit, H.: Permafrost is warming at a global scale, Nature Communications, 10, 264, https://doi.org/10.1038/s41467-018-08240-4, 2019.

Blaauw, M., and Christen, J. A.: Flexible paleoclimate age-depth models using an autoregressive gamma process, Bayesian Anal., 6, 457-474, https://doi.org/10.1214/11-BA618, 2011.

Blott, S. J., and Pye, K.: GRADISTAT: a grain size distribution and statistics package for the analysis of unconsolidated sediments, Earth Surface Processes and Landforms, 26, 1237-1248, https://doi.org/10.1002/esp.261, 2001.

Bosikov, N.: Wetness variability and dynamics of thermokarst processes in Central Yakutia, Proceedings of the 7th International Permafrost Conference, 1998, 71-74, 1998.

Brosius, L., Walter Anthony, K., Grosse, G., Chanton, J., Farquharson, L., Overduin, P. P., and Meyer, H.: Using the deuterium isotope composition of permafrost meltwater to constrain thermokarst lake contributions to atmospheric CH4 during the last deglaciation, Journal of Geophysical Research: Biogeosciences, 117, https://doi.org/10.1029/2011JG001810, 2012.

Butler, R. F.: Paleomagnetism: magnetic domains to geologic terranes, Blackwell Scientific Publications Boston, 1992.

Cole, J. J., Cole, J. J., Caraco, N. F., and Caraco, N. F.: Carbon in catchments: connecting terrestrial carbon losses with aquatic metabolism, Marine and Freshwater Research, 52, 101-110, https://doi.org/10.1071/MF00084, 2001.

Coplen, T. B., Brand, W. A., Gehre, M., Gröning, M., Meijer, H. A. J., Toman, B., and Verkouteren, R. M.: New Guidelines for δ13C Measurements, Anal. Chem., 78, 2439-2441, https://doi.org/10.1021/ac052027c, 2006.

Crate, S., Ulrich, M., Habeck, J. O., Desyatkin, A. R., Desyatkin, R. V., Fedorov, A. N., Hiyama, T., Iijima, Y., Ksenofontov, S., Mészáros, C., and Takakura, H.: Permafrost livelihoods: A transdisciplinary review and analysis of thermokarst-based systems of indigenous land use, Anthropocene, 18, 89-104, https://doi.org/10.1016/j.ancene.2017.06.001, 2017.

Dearing, J.: Magnetic susceptibility, Environmental magnetism: A practical guide, 6, 35-62, 1999.

Diekmann, B., Pestryakova, L., Nazarova, L., Subetto, D., Tarasov, P. E., Stauch, G., Thiemann, A., Lehmkuhl, F., Biskaborn, B., and Kuhn, G. J. P.: Late Quaternary lake dynamics in the Verkhoyansk Mountains of Eastern Siberia: implications for climate and glaciation history, Polarforschung, 86, 97-110, https://doi.org/10.2312/polarforschung.86.2.97, 2017.

Diochon, A., and Kellman, L.: Natural abundance measurements of 13C indicate increased deep soil carbon mineralization after forest disturbance, Geophysical Research Letters, 35, https://doi.org/10.1029/2008GL034795, 2008.

Fedorov, A., and Konstantinov, P.: Observations of surface dynamics with thermokarst initiation, Yukechi site, Central Yakutia, Proceedings of the 8th International Conference on Permafrost, 21-25 July 2003, Zurich, Switzerland, 2003a, 239-243,

Fedorov, A. N., and Konstantinov, P.: Observations of surface dynamics with thermokarst initiation, Yukechi site, Central Yakutia, 8th International Conference On Permafrost, Zurich, Switzerland, 2003b,

Fedorov, A. N.: Present post-disturbance dynamics of permafrost in Central Yakutia, Symptom of Environmental Change in Siberian Permafrost Region, 225-231, 2006.

French, H., and Shur, Y.: The principles of cryostratigraphy, Earth-Science Reviews, 101, 190-206, https://doi.org/10.1016/j.earscirev.2010.04.002, 2010.

Grosse, G., Jones, B., and Arp, C.: 8.21 Thermokarst Lakes, Drainage, and Drained Basins, in: Treatise on Geomorphology, edited by: Shroder, J. F., Academic Press, San Diego, 325-353, 2013.

Horita, J., Ueda, A., Mizukami, K., and Takatori, I.: Automatic δD and δ18O analyses of multi-water samples using H2- and CO2-water equilibration methods with a common equilibration set-up, International Journal of Radiation Applications and Instrumentation. Part A. Applied Radiation and Isotopes, 40, 801-805, https://doi.org/10.1016/0883-2889(89)90100-7, 1989.

Hugelius, G., Strauss, J., Zubrzycki, S., Harden, J. W., Schuur, E. a. G., Ping, C. L., Schirrmeister, L., Grosse, G., Michaelson, G. J., Koven, C. D., O'Donnell, J. A., Elberling, B., Mishra, U., Camill, P., Yu, Z., Palmtag, J., and Kuhry, P.: Estimated stocks of circumpolar permafrost carbon with quantified uncertainty ranges and identified data gaps, Biogeosciences (Online), 11, https://doi.org/10.5194/bg-11-6573-2014, 2014.

Huh, Y., Tsoi, M.-Y., Zaitsev, A., and Edmond, J. M.: The fluvial geochemistry of the rivers of Eastern Siberia: I. tributaries of the Lena River draining the sedimentary platform of the Siberian Craton, Geochimica et Cosmochimica Acta, 62, 1657-1676, https://doi.org/10.1016/S0016-7037(98)00107-0, 1998.

IPCC: Summary for Policymakers, IPCC Special Report on the Ocean and Cryosphere in a Changing Climate [H.-O. Pörtner, D.C. Roberts, V. Masson-Delmotte, P. Zhai, M. Tignor, E. Poloczanska, K. Mintenbeck, M. Nicolai, A. Okem, J. Petzold, B. Rama, N. Weyer (eds.)], In press, 2019.

Iwahana, G., Takano, S., Petrov, R. E., Tei, S., Shingubara, R., Maximov, T. C., Fedorov, A. N., Desyatkin, A. R., Nikolaev, A. N., Desyatkin, R. V., and Sugimoto, A.: Geocryological characteristics of the upper permafrost in a tundra-forest transition of the Indigirka River Valley, Russia, Polar Science, 8, 96-113, https://doi.org/10.1016/j.polar.2014.01.005, 2014.

Johansson, M., Callaghan, T. V., Bosiö, J., Åkerman, H. J., Jackowicz-Korczynski, M., and Christensen, T. R.: Rapid responses of permafrost and vegetation to experimentally increased snow cover in sub-arctic Sweden, Environ. Res. Lett., 8, 035025, 2013.

Jongejans, L. L., Strauss, J., Lenz, J., Peterse, F., Mangelsdorf, K., Fuchs, M., and Grosse, G.: Organic matter characteristics in yedoma and thermokarst deposits on Baldwin Peninsula, west Alaska, Biogeosciences, 15, 6033-6048, https://doi.org/10.5194/bg-15-6033-2018, 2018.

Kuznetsova, L. V., Zakharova, V. I., Sosina, N. K., Nikolin, E. G., Ivanova, E. I., Sofronova, E. V., Poryadina, L. N., Mikhalyova, L. G., Vasilyeva, I. I., Remigailo, P. A., Gabyshev, V. A., Ivanova, A. P., and Kopyrina, L. I.: Flora of Yakutia: Composition and Ecological Structure, in: The Far North: Plant Biodiversity and Ecology of Yakutia, edited by: Troeva, E. I., Isaev, A. P., Cherosov, M. M., and Karpov, N. S., Springer Netherlands, Dordrecht, 24-140, 2010.

Meyer, H., Schönicke, L., Wand, U., Hubberten, H. W., and Friedrichsen, H.: Isotope studies of hydrogen and oxygen in ground ice-experiences with the equilibration technique, Isotopes in Environmental and Health Studies, 133-149, https://doi.org/10.1080/10256010008032939, 2000.

Morgenstern, A., Grosse, G., Günther, F., Fedorova, I., and Schirrmeister, L. J. T. C. D.: Spatial analyses of thermokarst lakes and basins in Yedoma landscapes of the Lena Delta, The Cryosphere Discussions, 5, 1495-1545, https://doi.org/10.5194/tcd-5-1495-2011, 2011.

https://doi.org/10.5194/bg-2019-470
Preprint. Discussion started: 3 January 2020

Murton, J. B., Edwards, M. E., Lozhkin, A. V., Anderson, P. M., Savvinov, G. N., Bakulina, N., Bondarenko, O. V., Cherepanova, M. V., Danilov, P. P., Boeskorov, V., Goslar, T., Grigoriev, S., Gubin, S. V., Korzun, J. A., Lupachev, A. V., Tikhonov, A., Tsygankova, V. I., Vasilieva, G. V., and Zanina, O. G.: Preliminary paleoenvironmental analysis of permafrost deposits at Batagaika megaslump, Yana Uplands, northeast Siberia, Quaternary Research, 87, 314-330, https://doi.org/10.1017/qua.2016.15, 2017.

Nazarova, L., Lüpfert, H., Subetto, D., Pestryakova, L., and Diekmann, B.: Holocene climate conditions in central Yakutia (Eastern Siberia) inferred from sediment composition and fossil chironomids of Lake Temje, Quaternary International, 290-291, 264-274, https://doi.org/10.1016/j.quaint.2012.11.006, 2013.

Pye, K.: The nature, origin and accumulation of loess, Quaternary Science Reviews, 14, 653-667, https://doi.org/10.1016/0277-3791(95)00047-X, 1995.

Reimer, P. J., Bard, E., Bayliss, A., Beck, J. W., Blackwell, P. G., Ramsey, C. B., Buck, C. E., Cheng, H., Edwards, R. L., Friedrich, M., Grootes, P. M., Guilderson, T. P., Haflidason, H., Hajdas, I., Hatté, C., Heaton, T. J., Hoffmann, D. L., Hogg, A. G., Hughen, K. A., Kaiser, K. F., Kromer, B., Manning, S. W., Niu, M., Reimer, R. W., Richards, D. A., Scott, E. M., Southon, J. R., Staff, R. A., Turney, C. S. M., and Plicht, J. v. d.: IntCal13 and Marine13 Radiocarbon Age Calibration Curves 0–50,000 Years cal BP, Radiocarbon, 55, 1869-1887, https://doi.org/10.2458/azu_js_rc.55.16947, 2013.

Reineck, H.-E., and Singh, I. B.: Depositional sedimentary environments, 2nd ed., Springer-Verlag New York Berlin Heidelberg, 1980.

Reineck, H. E., and Singh, I. B.: Depositional Sedimentary Environments: With Reference to Terrigenous Clastics, Springer Science & Business Media, 566 pp., 2012.

Schirrmeister, L., Froese, D., Tumskoy, V., Grosse, G., and Wetterich, S.: Yedoma: Late Pleistocene ice-rich syngenetic permafrost of Beringia, in: Encyclopedia of Quaternary Science, 2 ed., Elsevier, 542-552, 2013.

Schuur, E. A. G., Bockheim, J., Canadell, J. G., Euskirchen, E., Field, C. B., Goryachkin, S. V., Hagemann, S., Kuhry, P., Lafleur, P. M., Lee, H., Mazhitova, G., Nelson, F. E., Rinke, A., Romanovsky, V. E., Shiklomanov, N., Tarnocai, C., Venevsky, S., Vogel, J. G., and Zimov, S. A.: Vulnerability of Permafrost Carbon to Climate Change: Implications for the Global Carbon Cycle, BioScience, 58, 701-714, https://doi.org/10.1641/B580807, 2008.

Schuur, E. A. G., McGuire, A. D., Schädel, C., Grosse, G., Harden, J. W., Hayes, D. J., Hugelius, G., Koven, C. D., Kuhry, P., Lawrence, D. M., Natali, S. M., Olefeldt, D., Romanovsky, V. E., Schaefer, K., Turetsky, M. R., Treat, C. C., and Vonk, J. E.: Climate change and the permafrost carbon feedback, Nature, 520, 171, https://doi.org/10.1038/nature14338, 2015.

Shmelev, D., Veremeeva, A., Kraev, G., Kholodov, A., Spencer, R. G. M., Walker, W. S., and Rivkina, E.: Estimation and Sensitivity of Carbon Storage in Permafrost of North-Eastern Yakutia, Permafrost and Periglacial Processes, 28, 379-390, https://doi.org/10.1002/ppp.1933, 2017.

Siewert, M. B., Hanisch, J., Weiss, N., Kuhry, P., Maximov, T. C., and Hugelius, G.: Comparing carbon storage of Siberian tundra and taiga permafrost ecosystems at very high spatial resolution, Journal of Geophysical Research: Biogeosciences, 120, 1973-1994, https://doi.org/10.1002/2015JG002999, 2015.

Soloviev, P.: Guidebook: alass thermokarst relief of central Yakutia, Second International Conference on Permafrost, Yakutsk, 1973, 13-28, 1973.

Stevenson, F. J.: Humus chemistry: genesis, composition, reactions, John Wiley & Sons, 1994.

Strauss, J., Schirrmeister, L., Wetterich, S., Borchers, A., and Davydov, S. P.: Grain-size properties and organic-carbon stock of Yedoma Ice Complex permafrost from the Kolyma lowland, northeastern Siberia, Global Biogeochemical Cycles, 26, https://doi.org/doi:10.1029/2011GB004104, 2012.

Strauss, J., Schirrmeister, L., Grosse, G., Wetterich, S., Ulrich, M., Herzschuh, U., and Hubberten, H.-W.: The deep permafrost carbon pool of the Yedoma region in Siberia and Alaska, Geophysical Research Letters, 40, 6165-6170, https://doi.org/10.1002/2013GL058088, 2013.

Strauss, J., Schirrmeister, L., Mangelsdorf, K., Eichhorn, L., Wetterich, S., and Herzschuh, U.: Organic-matter quality of deep permafrost carbon – a study from Arctic Siberia, Biogeosciences, 12, 2227-2245, https://doi.org/10.5194/bg-12-2227-2015, 2015.

Strauss, J., Schirrmeister, L., Grosse, G., Fortier, D., Hugelius, G., Knoblauch, C., Romanovsky, V., Schädel, C., Schneider von Deimling, T., Schuur, E. A. G., Shmelev, D., and Veremeeva, A.: Deep Yedoma permafrost: A synthesis of depositional characteristics and carbon vulnerability, Earth-Science Reviews, 75-86, https://doi.org/10.1016/j.earscirev.2017.07.007, 2017.

Ulrich, M., Grosse, G., Strauss, J., and Schirrmeister, L.: Quantifying Wedge-Ice Volumes in Yedoma and Thermokarst Basin Deposits, Permafrost and Periglacial Processes, 25, 151-161, https://doi.org/10.1002/ppp.1810, 2014.

Ulrich, M., Matthes, H., Schirrmeister, L., Schütze, J., Park, H., Iijima, Y., and Fedorov, A. N.: Differences in behaviour and distribution of permafrost-related lakes in Central Yakutia and their response to climatic drivers, Water Resources Research, 1167-1188, https://doi.org/10.1002/2016WR019267, 2017a.

Ulrich, M., Wetterich, S., Rudaya, N., Frolova, L., Schmidt, J., Siegert, C., Fedorov, A. N., and Zielhofer, C.: Rapid thermokarst evolution during the mid-Holocene in Central Yakutia, Russia, The Holocene, 27, 1899-1913, https://doi.org/10.1177/0959683617708454, 2017b.

Ulrich, M., Matthes, H., Schmidt, J., Fedorov, A. N., Schirrmeister, L., Siegert, C., Schneider, B., Strauss, J., and Zielhofer, C.: Holocene thermokarst dynamics in Central Yakutia - A multi-core and robust grain-size endmember modeling approach, Quaternary Science Reviews, 218, https://doi.org/10.1016/j.quascirev.2019.06.010, 2019.

Vonk, J. E., Mann, P. J., Davydov, S., Davydova, A., Spencer, R. G. M., Schade, J., Sobczak, W. V., Zimov, N., Zimov, S., Bulygina, E., Eglinton, T. I., and Holmes, R. M.: High biolability of ancient permafrost carbon upon thaw, Geophysical Research Letters, 40, 2689-2693, https://doi.org/doi:10.1002/grl.50348, 2013.

Walter Anthony, K. M., Zimov, S. A., Grosse, G., Jones, M. C., Anthony, P. M., Iii, F. S. C., Finlay, J. C., Mack, M. C., Davydov, S., Frenzel, P., and Frolking, S.: A shift of thermokarst lakes from carbon sources to sinks during the Holocene epoch, Nature, 511, 452, https://doi.org/10.1038/nature13560, 2014.

Weiss, N., Blok, D., Elberling, B., Hugelius, G., Jørgensen, C. J., Siewert, M. B., and Kuhry, P.: Thermokarst dynamics and soil organic matter characteristics controlling initial carbon release from permafrost soils in the Siberian Yedoma region, Sedimentary Geology, 340, 38-48, https://doi.org/10.1016/j.sedgeo.2015.12.004, 2016.

Wetterich, S., Herzschuh, U., Meyer, H., Pestryakova, L., Plessen, B., Lopez, C. M. L., and Schirrmeister, L.: Evaporation effects as reflected in freshwater and ostracod calcite from modern environments in Central and Northeast Yakutia (East Siberia, Russia), Hydrobiologia, 171-195, https://doi.org/10.1007/s10750-008-9505-y, 2008.

Wetterich, S., Schirrmeister, L., Andreev, A. A., Pudenz, M., Plessen, B., Meyer, H., and Kunitsky, V. V.: Eemian and Late Glacial/Holocene palaeoenvironmental records from permafrost sequences at the Dmitry Laptev Strait (NE Siberia, Russia), Palaeogeography, Palaeoclimatology, Palaeoecology, 279, 73-95, https://doi.org/10.1016/j.palaeo.2009.05.002, 2009.

https://doi.org/10.5194/bg-2019-470
Preprint. Discussion started: 3 January 2020

Wilcock, P. R., and Crowe, J. C.: Surface-based Transport Model for Mixed-Size Sediment, Journal of Hydraulic Engineering, 129, 120-128, https://doi.org/doi:10.1061/(ASCE)0733-9429(2003)129:2(120), 2003.

Windirsch, T., Grosse, G., Ulrich, M., Schirrmeister, L., Fedorov, A. N., Konstantinov, P., Fuchs, M., and Strauss, J.: Organic material, sediment and ice characteristics of two permafrost cores from Yukechi Alas, Central Yakutia, PANGAEA, https://doi.org/10.1594/PANGAEA.898754, 2019.

Yao, T., Li, Z., Thompson, L. G., Mosley-Thompson, E., Wang, Y., Tian, L., Wang, N., and Duan, K.: δ18O records from Tibetan ice cores reveal differences in climatic changes, Annals of Glaciology, 43, 1-7, https://doi.org/10.3189/172756406781812131, 2006.

Zhang, T., Barry, R. G., Knowles, K., Heginbottom, J. A., and Brown, J.: Statistics and characteristics of permafrost and ground-ice distribution in the Northern Hemisphere, Polar Geography, 23, 132-154, https://doi.org/10.1080/10889379909377670, 1999.

https://doi.org/10.5194/bg-2019-470
Preprint. Discussion started: 3 January 2020

Table 1 - Radiocarbon measurement data and calibrated ages for YED1 and Alas1 bulk organic material samples.

Core	Mean sample depth [cm bs]	^{14}C age [yr BP]	+/- [yr]	Calibrated ages (2 σ)* [cal yr BP]	Mean age [cal yr BP]	Core unit
YED1	157.5	18064	± 104	21582–22221	21890	Y1
	298	25973	± 88	29822–30640	30268	Y1
	589.5	35965	± 184	40116–41118	40608	Y1
	1636	49000	± 0	infinite age	> 49000	Y3
	1998.5	45854	± 501	48202–calib. limit	49232	Y4
Alas1	199	12826	± 57	15144–15548	15287	A1
	812.5	23615	± 151	27478–27976	27729	A2
	1530.5	42647	± 364	45172–46619	45870	A4
	1967.5	39027	± 251	42478–43262	42865	A4

* calibrated using Calib 7.1 (Stuiver et al., 2018) equipped with IntCal 13 (Reimer et al., 2013)

https://doi.org/10.5194/bg-2019-470
Preprint. Discussion started: 3 January 2020

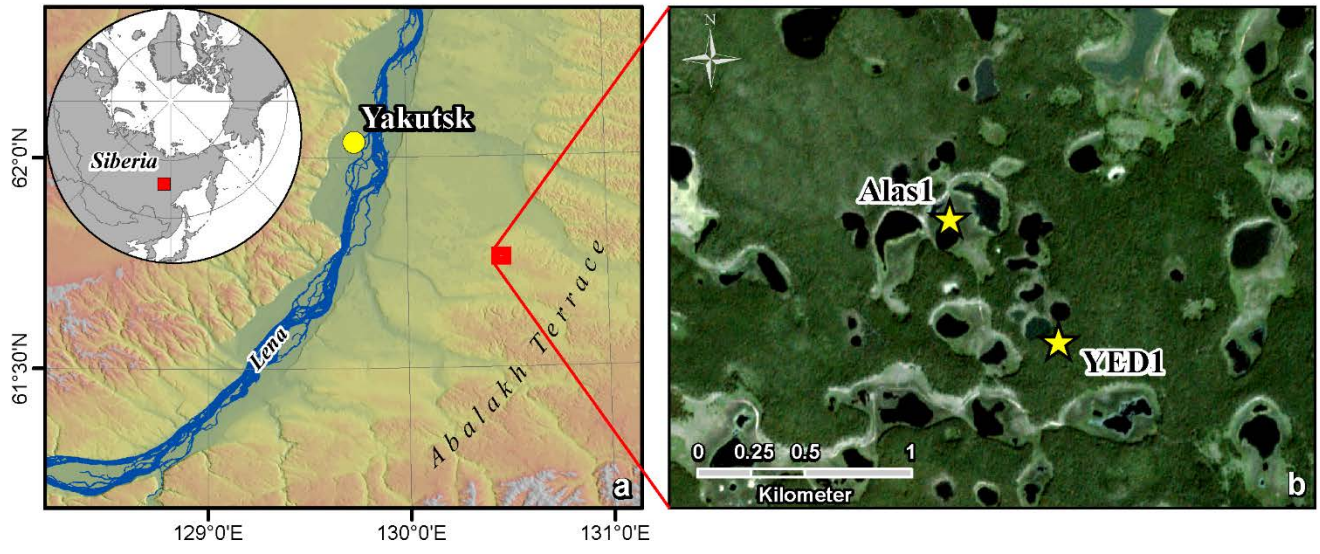

Figure 1 – Study site overview; a: location of the Yukechi Alas study site in Central Yakutia on the edge of the Abalakh Terrace; b: locations of the Alas1 and the YED1 coring sites within the Yukechi Alas landscape (Planet OrthoTile, acquisition date: 7 July 2018).

https://doi.org/10.5194/bg-2019-470
Preprint. Discussion started: 3 January 2020

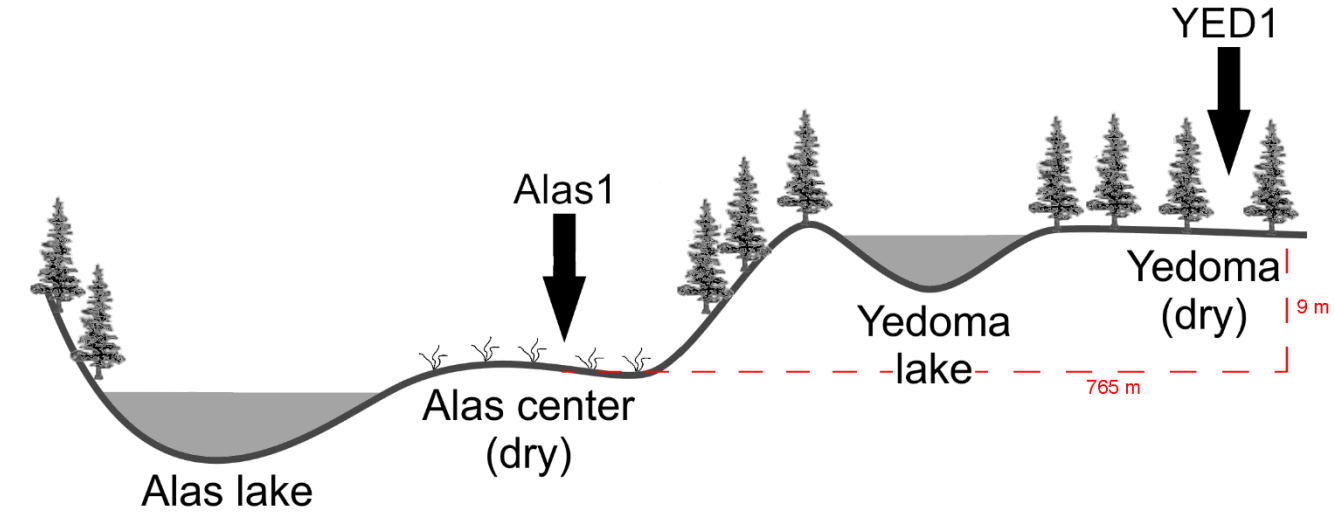

Figure 2 – Setting of the drilling locations for the Alas1 and YED1 cores showing distance and height difference between the locations (vertical scale exaggerated).

https://doi.org/10.5194/bg-2019-470
Preprint. Discussion started: 3 January 2020

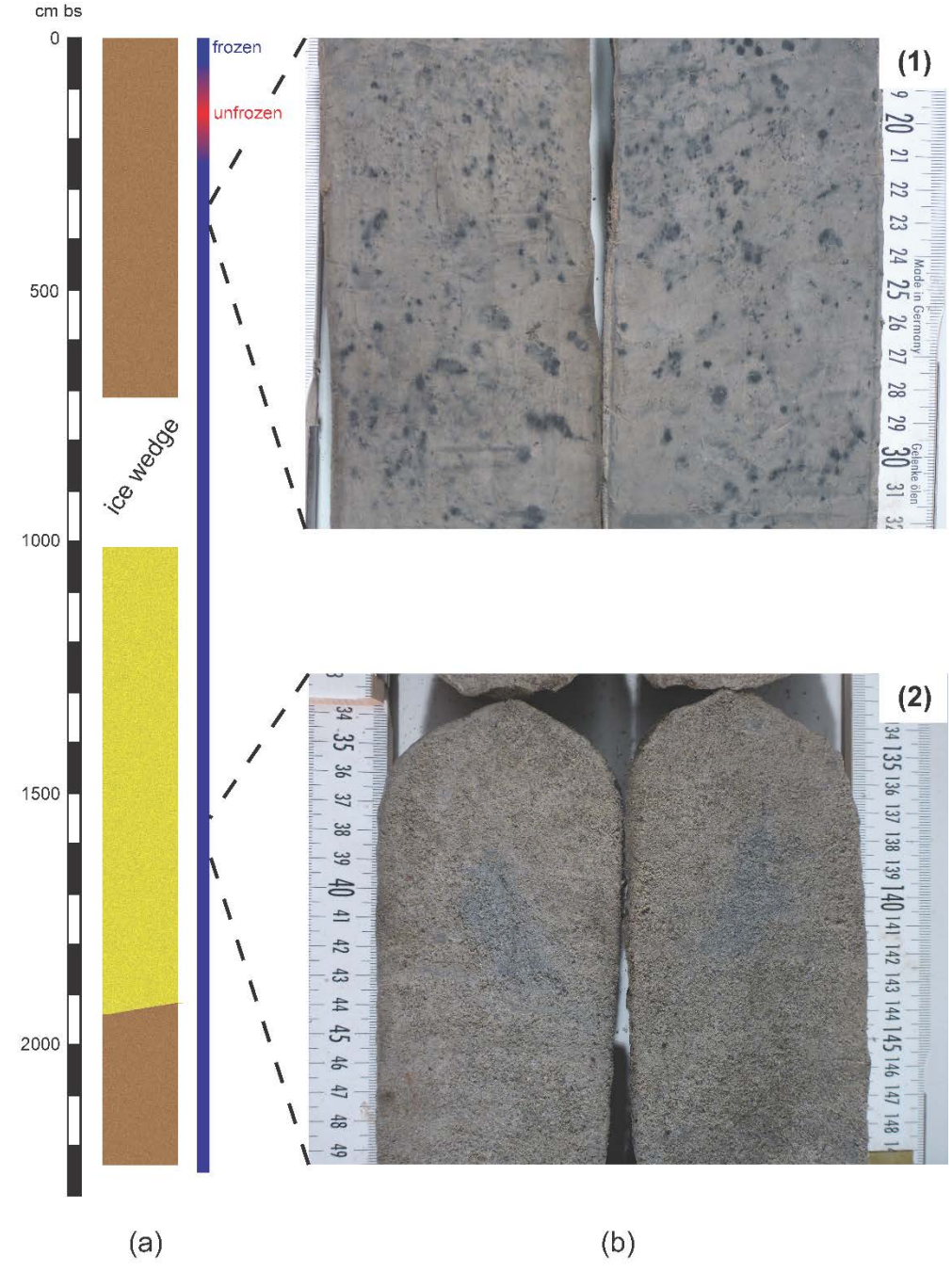

Figure 3 – a: overview of the Yedoma core; depth given in cm bs; state after core retrieval is given by colors: blue = frozen, red = unfrozen; location of the ice wedge is marked; brown marks silty sediments, yellow marks sandy sediments; b: detailed pictures of the YED1 core; (1) 317-332 cm bs, picture of Y1 showing black organic-rich inclusions

https://doi.org/10.5194/bg-2019-470
Preprint. Discussion started: 3 January 2020

within the grey silty matrix; (2) 1532-1549 cm bs, picture of Y3, showing the coarse sandy material with no visible cryostructures or organic material.

https://doi.org/10.5194/bg-2019-470
Preprint. Discussion started: 3 January 2020

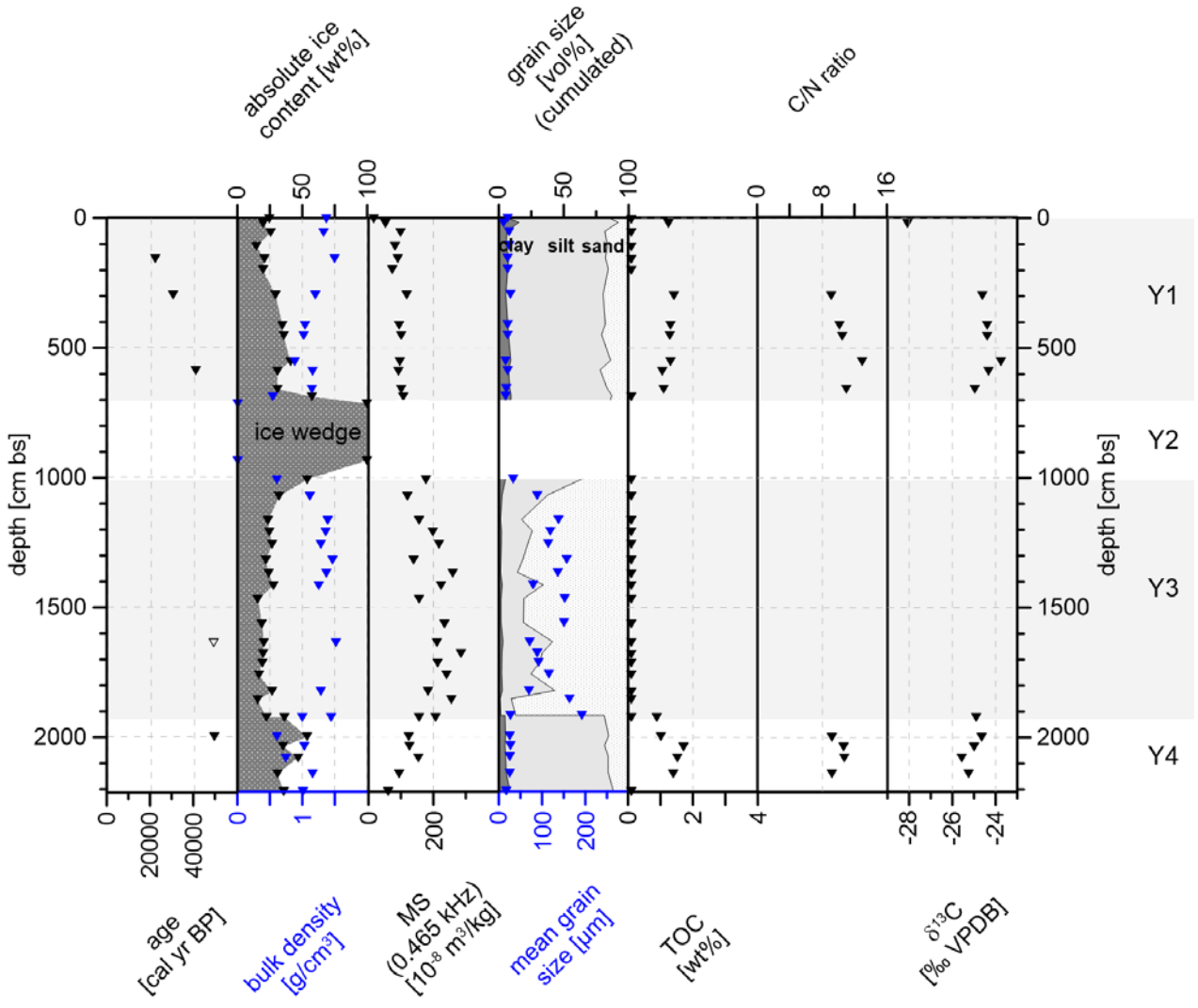

Figure 4 - Characteristics of the Yedoma core YED 1: radiocarbon age, absolute ice content, bulk density, MS, grain size composition, mean grain size, TOC, C/N ratio, and $\delta^{13}C$ ratio; hollow triangle indicates an infinite radiocarbon age; grey/white areas mark the different stratigraphic units (Y1 to Y4).

https://doi.org/10.5194/bg-2019-470
Preprint. Discussion started: 3 January 2020

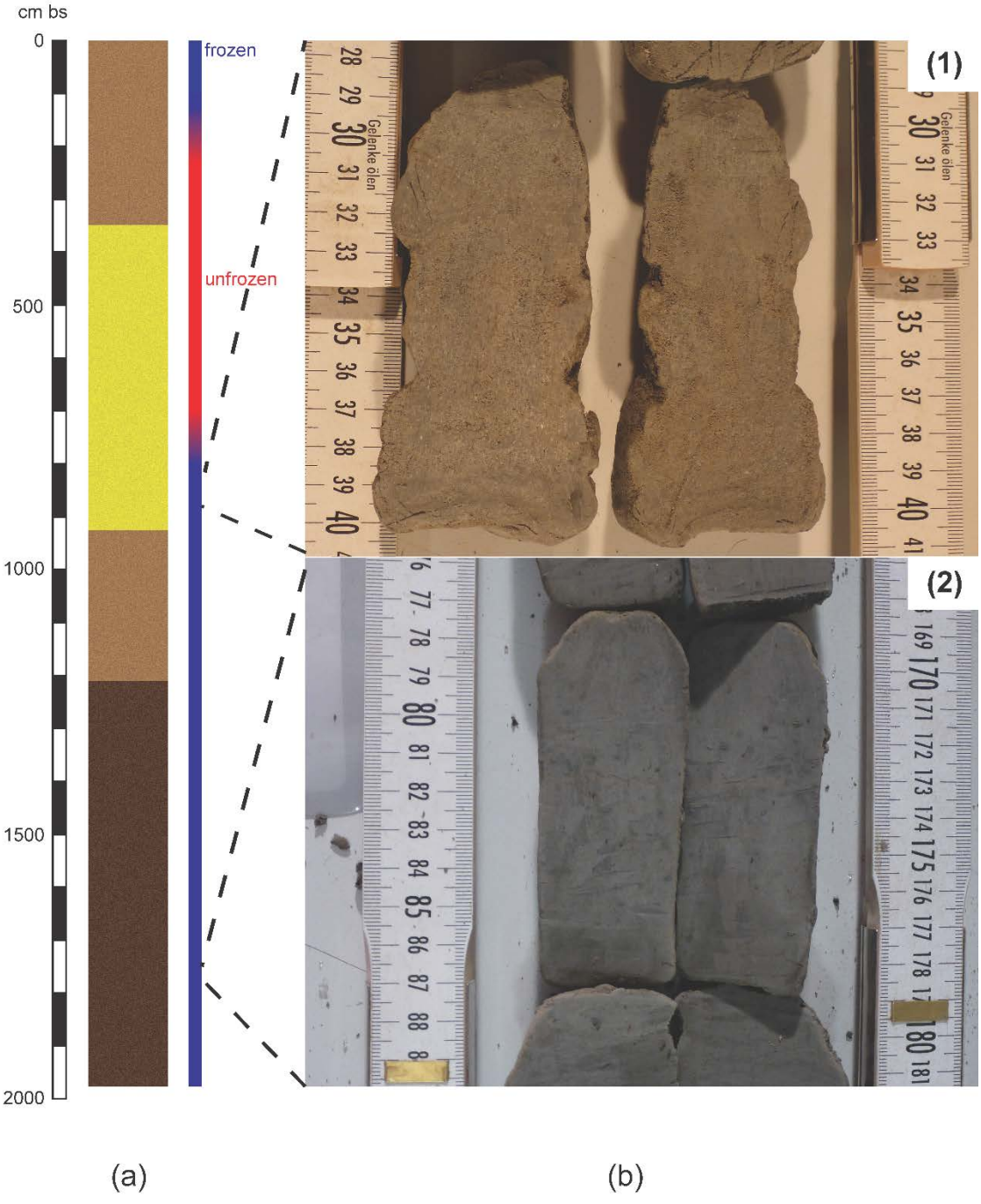

Figure 5 – a: overview of the Alas1 core; depth given in cm bs; state after core retrieval is given by colors: blue = frozen, red = unfrozen; light brown marks silty material, yellow marks sandy material, dark brown marks silty material

https://doi.org/10.5194/bg-2019-470
Preprint. Discussion started: 3 January 2020

containing more organic material; b: detailed pictures of the Alas1 core; (1) 828–840 cm bs picture of the sandy A2 unit; (2) 1767–1781 cm bs picture of the fine-grained silt-dominated A4 unit including black organic-rich inclusions.

https://doi.org/10.5194/bg-2019-470
Preprint. Discussion started: 3 January 2020

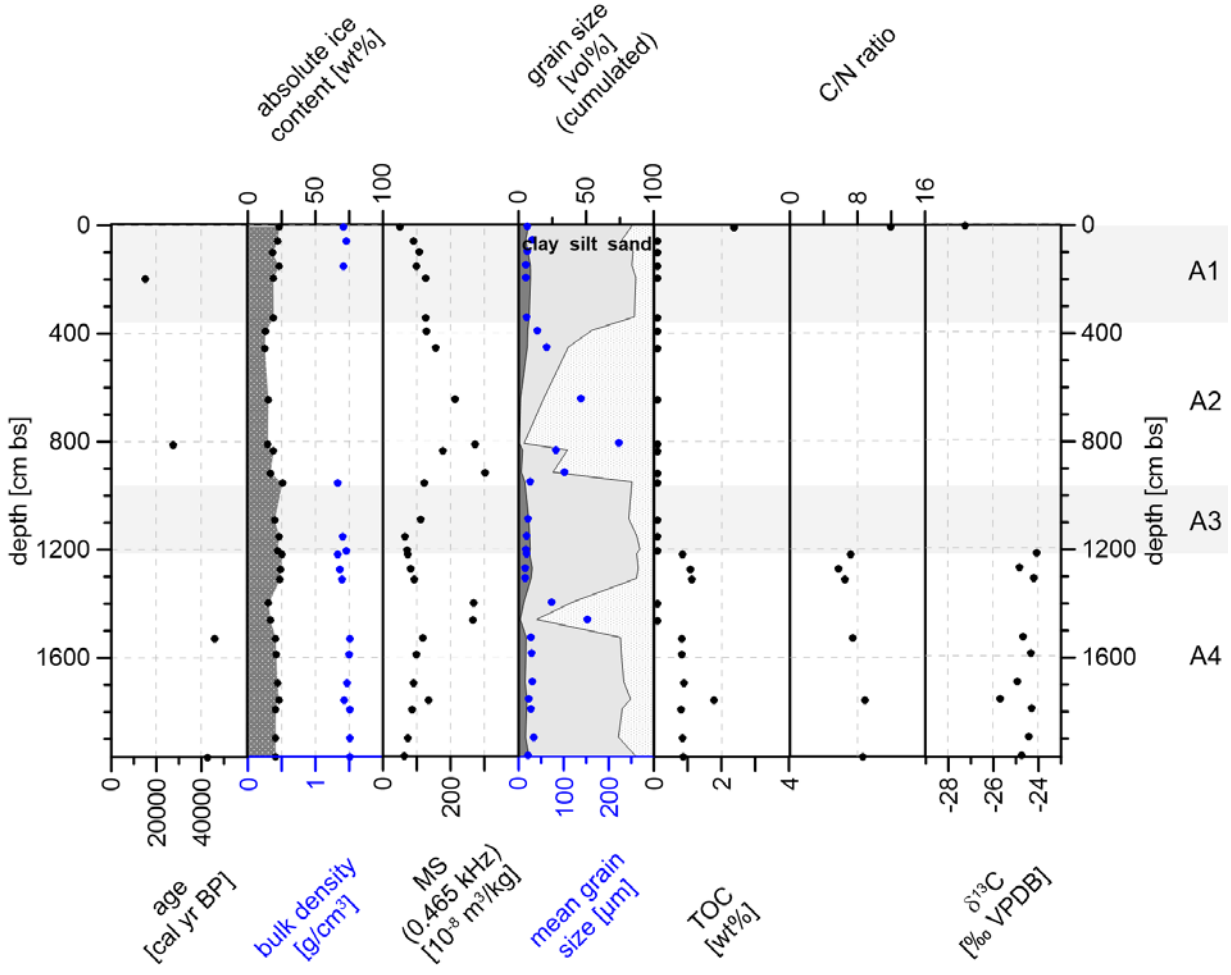

Figure 6 - Characteristics of the Alas1 core: radiocarbon age, absolute ice content, bulk density, MS, grain size composition, mean grain size, TOC, C/N ratio, and $\delta^{13}C$ ratio; grey/white areas mark the different stratigraphic units (A1 to A4).

https://doi.org/10.5194/bg-2019-470
Preprint. Discussion started: 3 January 2020

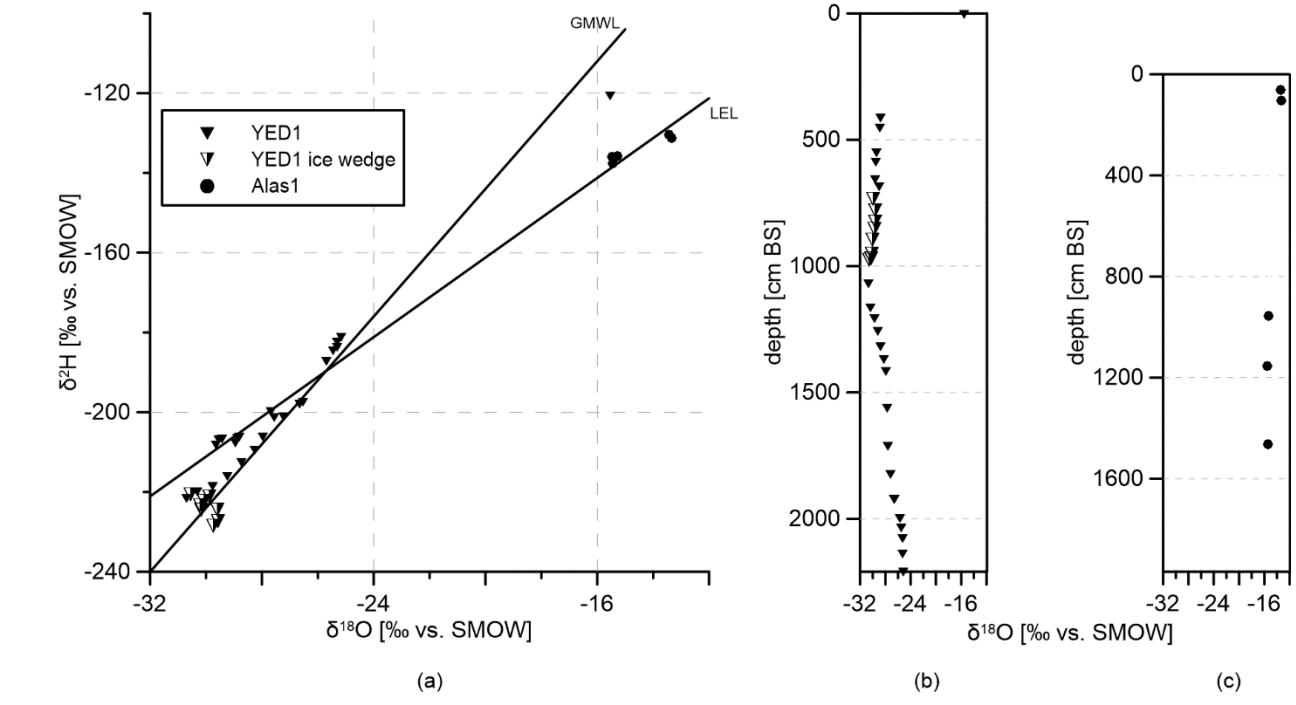

Figure 7 – The characteristics of water stable isotopes in the studied sediment cores; a: stable hydrogen and oxygen isotope ratios of YED1 pore ice (black triangles), YED1 ice wedge ice (semi-hollow triangles), and Alas1 pore ice and pore water (black dots) [‰ vs. SMOW]; global meteoric water line GMWL: y=8x; local evaporation line LEL of Central Yakutia (based on data compiled until 2005 after Wetterich et al., 2008); b and c: oxygen isotopes of YED1 (b) and Alas1 (c) plotted over depth.